Membrane conductances of mouse cone photoreceptors

Norianne T. Ingram[1,2] ⓘ, Alapakkam P. Sampath[2] ⓘ, and Gordon L. Fain[1,2] ⓘ

Vertebrate photoreceptor cells respond to light through a closure of CNG channels located in the outer segment. Multiple voltage-sensitive channels in the photoreceptor inner segment serve to transform and transmit the light-induced outer-segment current response. Despite extensive studies in lower vertebrates, we do not know how these channels produce the photoresponse of mammalian photoreceptors. Here we examined these ionic conductances recorded from single mouse cones in unlabeled, dark-adapted retinal slices. First, we show measurements of the voltage dependence of the light response. After block of voltage-gated Ca^{2+} channels, the light-dependent current was nearly linear within the physiological range of voltages with constant chord conductance and a reversal potential similar to that previously determined in lower vertebrate photoreceptors. At a dark resting membrane potential of −45 mV, cones maintain a standing Ca^{2+} current (i_{Ca}) between 15 and 20 pA. We characterized the time and voltage dependence of i_{Ca} and a calcium-activated anion channel. After constitutive closure of the CNG channels by the nonhydrolysable analogue GTP-γ-S, we observed a light-dependent increase in i_{Ca} followed by a Ca^{2+}-activated K^+ current, both probably the result of feedback from horizontal cells. We also recorded the hyperpolarization-activated cyclic nucleotide-gated (HCN) conductance (i_h) and measured its current–voltage relationship and reversal potential. With small hyperpolarizations, i_h activated with a time constant of 25 ms; activation was speeded with larger hyperpolarizations. Finally, we characterized two voltage-gated K^+-conductances (i_K). Depolarizing steps beginning at −10 mV activated a transient, outwardly rectifying i_K blocked by 4-AP and insensitive to TEA. A sustained i_K isolated through subtraction was blocked by TEA but was insensitive to 4-AP. The sustained i_K had a nearly linear voltage dependence throughout the physiological voltage range of the cone. Together these data constitute the first comprehensive study of the channel conductances of mouse photoreceptors.

Introduction

Photoreceptors are tasked with detecting and encoding photon absorption. To do this reliably, they use a heterotrimeric G-protein cascade (Yau and Hardie, 2009; Arshavsky and Burns, 2012; Fain, 2019). Light stimulates visual pigment, which activates a phosphodiesterase, decreases the outer-segment cGMP concentration, and closes CNG cation-permeant channels, leading to a hyperpolarizing voltage response. Voltage-gated channels located in the inner segment (see Van Hook et al., 2019) respond to these changes in membrane potential (V_m) and alter the waveform of the response. Finally, the light-induced hyperpolarization of V_m decreases the influx of Ca^{2+} at synaptic ribbons and suppresses the release of glutamate into the synaptic cleft (Copenhagen and Jahr, 1989; Johnson et al., 2007; Choi et al., 2008).

To date, no study has used voltage-clamp recording to make a systematic characterization of the properties of ion channels in dark-adapted mouse photoreceptors. These measurements are important, because they are essential to our understanding of how the photocurrent in the outer segment is shaped by conductances in the inner segment. Cones are of particular interest because of their high density in the human fovea and their importance for visual detection over most of the operating range of human vision. Recordings from mouse are especially useful because outer and inner segment conductances can be modified or eliminated in transgenic animals. Previously, our understanding of mouse cone physiology has been hindered by the difficulty of making single-cell recordings, in part from the scarcity of cones, which constitute ~3% of the photoreceptors in the mouse retina (Jeon et al., 1998). We have recently shown that these difficulties can by surmounted by making whole-cell patch clamp recordings from unlabeled cones in mouse with a frequency of success and signal-to-noise sufficiently high to

[1]Department of Integrative Biology and Physiology, University of California, Los Angeles, CA;   [2]Department of Ophthalmology and Jules Stein Eye Institute, University of California, Los Angeles, CA.

Correspondence to Gordon L. Fain: gfain@ucla.edu.

analyze the biophysical properties of the cone response (Ingram et al., 2019). We have combined our method with the use of specific voltage manipulations and pharmacological agents to identify and characterize the major ionic conductances in mammalian cones.

Materials and methods

Animals

Experiments were performed in accordance with rules and regulations of the National Institutes of Health guidelines for research animals, as approved by the Institutional Animal Care and Use Committee of the University of California, Los Angeles (Los Angeles, CA). Mice were kept under cyclic light (12 on/12 off) with ad libitum food and water in approved cages. Male and female mice were used in approximately equal numbers and were between 2 and 6 mo of age.

Experiments were performed on cones with genetic mutations that limit the contribution of rods (Ingram et al., 2019). Most recordings were obtained from mice lacking the gap junction protein connexin36 ($Cx36^{-/-}$), which have the additional advantage of removing signal spread from the recorded cell. $Cx36^{-/-}$ mice were generated by D. Paul (Harvard University, Boston, MA; Deans et al., 2002) and obtained from S. Wu (Baylor College of Medicine, Houston, TX). In Fig. 1, A and B, recordings are shown from mice in which the rod-specific α subunit of the G-protein transducin had been deleted ($Gnat1^{-/-}$). These mice were originally made in the laboratory of J. Lem (Tufts University, Boston, MA; Calvert et al., 2000) and were obtained locally from the laboratory of G. Travis (University of California, Los Angeles, Los Angeles, CA). Recordings from cones in $Gnat1^{-/-}$ mice displayed response characteristics that were indistinguishable from cones recorded in $Cx36^{-/-}$ mice.

Solutions

Mouse retinas were sliced in HEPES-buffered Ames' medium, which contained 2.38 g HEPES per liter and was balanced with 0.875 g NaCl per liter to give an osmolarity of 284 ± 1 mOsm (pH 7.35 ± 0.5). Ames'-HEPES was kept on ice and continuously bubbled with 100% O_2. Retinal slices were superfused at 2 ml/min in the recording chamber with Ames' medium, which was continuously bubbled with 95% O_2/5% CO_2 and buffered with 1.9 g per liter sodium bicarbonate to maintain pH between 7.3 and 7.4. The ion concentrations of the principal ions in Ames' medium (in mM) are as follows (Ames and Nesbett, 1981): Na^+, 143; K^+, 3.6; Ca^{2+}, 2.3; Mg^{2+}, 2.4; Cl^-, 125.4; HCO_3^-, 22.6; and SO_4^{2-}, 2.4. In some experiments, channel-blocking compounds were added to the external solution (Van Hook et al., 2019). These compounds and their applied concentrations are as follows: isradipine (10 µM; ISR; Sigma) to block L-type voltage-dependent Ca^{2+} channels at the photoreceptor synaptic terminal; iberiotoxin (100 nM, IBX, Tocris) to block Ca^{2+}-activated (BK) K⁺ channels; niflumic acid (100–250 µM, NFA, Sigma), to block Ca^{2+}-activated Cl⁻ channels; TEA (25 mM, Sigma), to block sustained voltage-dependent K^+ channels; and 4-aminopyridine (2 mM, 4-AP, Sigma), to block transient voltage-dependent K^+ channels.

The standard internal solution for recording pipettes was a potassium aspartate (K-Asp) solution consisting of (in mM) 125 K-Asp, 10 KCl, 10 HEPES, 5 NMDG-HEDTA, 0.5 $CaCl_2$, 0.5 $MgCl_2$, 0.1 ATP-Mg, 0.5 GTP-Tris, and 2.5 NADPH (pH 7.3 ± 0.02 with NMDG-OH; 280 ± 1 mOsm). NMDG is N-methyl-D-glucamine, and HEDTA is N-(2-hydroxyethyl)-ethylenediamine-N-N'-N'-triacetic acid. The calculated free-Ca^{2+} concentration of this solution was 5×10^{-7} M. In the experiments of Fig. 3, 2 mM GTP-γ-S (Sigma) was added to the K-Asp internal to produce constitutive activation of the cone G protein transducin and maintain closure of CNG channels. In several experiments, the internal solution was changed to a cesium methane–sulfonate solution consisting of (in mM) 110 $CsCH_3O_3S$, 12 TEA-Cl, 10 HEPES, 10 EGTA, 2 QX-314-Br, 11 ATP-Mg, 0.5 GTP-Tris, 0.5 $MgCl_2$, and 1 NAD^+ (pH 7.3 with CsOH; 280 ± 1 mOsm). The calculated free-Ca^{2+} concentration of this solution was $<10^{-9}$ M. This solution was used to block potassium conductances including the hyperpolarization-activated and cyclic nucleotide-gated (HCN) current i_h (Fain et al., 1978; Yagi and Macleish, 1994). All values of cone V_m have been corrected by subtracting the liquid junction potential (Neher, 1992), which was measured to be 10 mV for these internal solutions.

Whole-cell patch clamp in retinal slices

The procedure for making whole-cell recordings from mouse cones was previously described (Ingram et al., 2019). In brief, mice were sacrificed by cervical dislocation after overnight dark adaptation. The anterior portion of the eye including the lens was removed, and the remaining eyecup was stored at 32°C in a custom, light-tight storage container that allowed for the gassing of solutions. For each slice preparation, half of the eyecup was isolated with a #10 scalpel, and the retina was gently separated from the retinal pigmented epithelium with fine tweezers. The isolated retinal piece was embedded in 3% of low-temperature-gelling agar in Ames'-HEPES. In cold Ames'-HEPES, 200-µm-thick slices were cut with a vibratome (Leica VT-1000S); the retina was cut vertically in an attempt to maintain neural circuitry. Cut slices were either transferred to dishes for immediate recording or stored in the light-tight container with the remaining pieces of the eyecups. During recordings, slices were stabilized with handmade anchors, and the bath solution was maintained at 35 ± 1°C. Cones were identified by the position and appearance of their somata, as well as from measurements of membrane capacitance and sensitivity to a moderate-intensity flash (Ingram et al., 2019). All light stimuli were brief (3–5 ms), monochromatic flashes of 405-nm light, a value near the isosbestic point of the S-cone and M-cone pigments (Nikonov et al., 2006). Monochromatic light was provided by ultra-bright light-emitting diodes driven with a linear feedback driver (Opto-LED; Carin Research). Light intensity was calibrated and converted into cone pigment molecules bleached (P*) from a collecting area of 0.013 µm², as previously described (Ingram et al., 2019). Protocols for measuring the reversal potential of the photoresponse and the voltage dependence of other inner-segment membrane currents, including methods of leak subtraction, are given for each of the experiments in the Results section and in the figure legends. Responses were filtered at 500 Hz
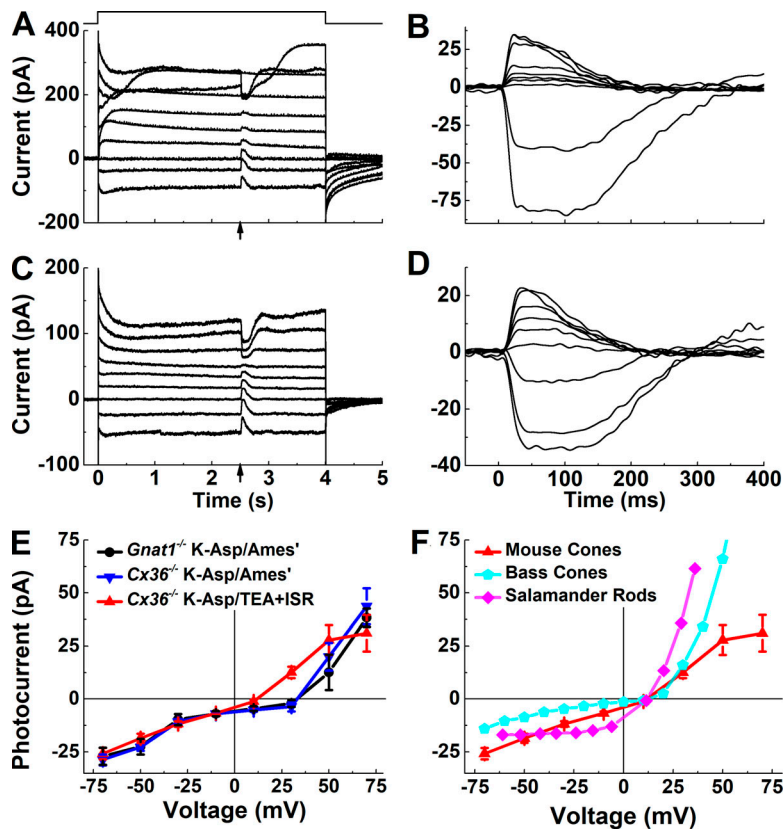
Ingram et al.
Conductances of mouse cone photoreceptors

Journal of General Physiology
https://doi.org/10.1085/jgp.201912520

2 of 11

Figure 1. **Reversal of mouse cone photocurrent. (A–D)** Whole-cell patch recordings from *Gnat1*$^{-/-}$ mice (A and B) and from *Cx36*$^{-/-}$ mice (C and D). Holding potential was initially –50 mV and was changed to test potentials from –90 mV to +70 mV in 20-mV steps. Sample command step shown in A. At 2.5 s after the change in holding potential, the cones were stimulated with a saturating flash bleaching 1.2×10^4 P* (arrows). The left column shows raw current traces. The right column shows photoresponses at each V_m overlaid after baseline subtraction. For C and D, 10 µM ISR and 25 mM TEA had been added to the bath solution. **(E)** Curves give peak amplitude of responses to the saturating flash as a function of holding potential, as follows: black circles, *Gnat1*$^{-/-}$, K-Asp internal, Ames' bicarbonate external ($n = 3$); blue inverted triangles, *Cx36*$^{-/-}$, K-Asp internal, Ames' bicarbonate external ($n = 8$); red triangles, *Cx36*$^{-/-}$, K-Asp internal, Ames' bicarbonate external with addition of 25 mM TEA and 10 µM ISR ($n = 8$). Data points are means ± SEM. **(F)** Comparison of mouse cone current-voltage curve (red triangles) to previous results of current-voltage curves from salamander rods (fuchsia diamonds) and bass (fish) cones (blue pentagons).

(eight-pole Bessel, Frequency Devices 900), sampled at 10 kHz, and recorded in an open-source, MATLAB-based program called Symphony Data Acquisition System (http://www.open-ephys.org/symphony/). Data were analyzed with custom scripts written in MATLAB.

Results

We have recently described a methodology that allows for reliable measurements of voltage-clamp currents with patch electrodes in retinal slices from single, dark-adapted mouse cones (Ingram et al., 2019). Cones can be identified without the use of fluorescent dyes or any other marking procedure, obviating the need to expose the photoreceptors to light before recording. Recordings can be made not only from dark-adapted WT cones but also from mutant mouse lines, in particular from *Gnat*$^{-/-}$ cones lacking rod input through rod/cone gap junctions, and from *Cx36*$^{-/-}$ cones, which lack gap junctions connecting cones to other photoreceptors (see Fain and Sampath, 2018). We have taken advantage of this preparation to investigate the properties of the membrane conductances of mammalian cone photoreceptors.

Voltage dependence and reversal potential of the cGMP-gated conductance

Although measurements of the voltage dependence and reversal potential of cGMP-gated (CNG) channels have been made from voltage clamp of intact amphibian rods (Baylor and Nunn, 1986) and fish cones (Miller and Korenbrot, 1993), no similar measurements have been made from mammalian photoreceptors. We

investigated the properties of the mouse cone photoresponse with the following protocol. Cones were held initially at –50 mV and then stepped to a new holding potential for 4 s from –70 mV to +70 mV in 20-mV increments. We allowed the baseline current at the new potential to stabilize for 2.5 s and then stimulated the cone with a bright 405-nm light flash, sufficiently intense to close transiently all of the CNG channels. We show the results of such an experiment on a *Gnat1*$^{-/-}$ cone in Fig. 1 A. Photoresponses from these records were isolated and overlaid after baseline subtraction in Fig. 1 B.

The current produced by light stimulation reversed at +27 ± 7 mV (mean ± SEM) in cones from *Gnat1*$^{-/-}$ retinas (Fig. 1 E, black lines and symbols). This value is more positive than previous measurements from amphibian rods or fish cones (Haynes and Yau, 1985; Baylor and Nunn, 1986; Miller and Korenbrot, 1993) or from olfactory receptors, which also use CNG channels (see for example Kurahashi, 1989). It is also much more positive than expected from the Goldman equation and the reported ion selectivity of expressed CNG channels (see Kaupp and Seifert, 2002). Moreover, the amplitude of the light-sensitive current decreased as the V_m was depolarized but seemed to "hesitate" near the reversal potential; it then suddenly became very large and inward when the potential was stepped to +50 mV. This suggested to us either that the V_m of the cone was not sufficiently space clamped, thereby preventing the entire cone from being isopotential at any command voltage, or that some change in current was contributing to the photoresponse in addition to that produced by closure of the CNG channels.

To test the possibility of some inadequacy in the space clamp, we repeated the experiment of Fig. 1, A and B, on $Cx36^{-/-}$ cones. Since these cones lack gap junctions between photoreceptors and are relatively small in dimension, they should be electrically compact and provide a sufficient space clamp of the totality of the cone. The light-sensitive current reversed at +31 ± 4 mV (Fig. 1 E, blue symbols and line), not significantly different from the value obtained from $Gnat1^{-/-}$ cones. Leakage of current from the recorded cell to other photoreceptors would therefore seem not to explain the very positive value of the reversal potential.

We next considered the possibility that some other change in current was produced by light stimulation and was contributing to the response, perhaps from an inner-segment conductance. Because our recordings were made from cones in intact retinal slices, our light flashes would have stimulated many surrounding photoreceptors in addition to the cone from which our recording was made. These photoreceptors could have been synapsing onto adjacent horizontal cells, which could be feeding back onto the recorded cone. Experiments from many laboratories on a variety of preparations (Verweij et al., 1996; reviewed in Thoreson and Mangel, 2012; Diamond, 2017), including mammalian cones (Packer et al., 2010), have shown that horizontal-cell feedback can change the voltage dependence of the photoreceptor Ca^{2+} current, effectively increasing the Ca^{2+} current and any currents activated by Ca^{2+} also present in the cone inner segment (see for example Verweij et al., 2003). We therefore remeasured the reversal potential of the cone photoresponse in the presence of 10 µM ISR to block the Ca^{2+} current and any currents modulated by an increase in Ca^{2+} influx. These measurements are shown in Fig. 1, C and D, and gave a reversal potential of +13 ± 2 mV (Fig. 1 E, red symbols and line). Exact values for permeability ratios could not be obtained, because nothing is presently known about the relative Ca^{2+} permeability of the CNG channels or the fraction of light-dependent current carried by Ca^{2+} for mammalian cones.

In Fig. 1 F, we compare the light-sensitive current of mouse cones in the physiological range of voltages with similar measurements from amphibian rods (Baylor and Nunn, 1986) and fish cones (Miller and Korenbrot, 1993; see also Haynes and Yau, 1985). For all of these receptors, the CNG channels have a similar reversal potential and presumably also a similar ion selectivity. Within the physiological range of V_m, mouse and bass cones have a nearly constant chord conductance with little dependence on voltage. This result is in striking contrast to measurements from amphibian rods (see Discussion and Baylor and Nunn, 1986).

Voltage-gated Ca^{2+} currents and Ca^{2+}-activated Cl^- currents
The experiments of Fig. 1 suggest that cones in our preparations have voltage-gated Ca^{2+} currents (Yagi and Macleish, 1994; Taylor and Morgans, 1998; DeVries and Schwartz, 1999), which can be blocked by ISR and are likely to be L-type $Ca_V1.4$ channels known to be responsible for synaptic transmission in mammalian photoreceptors (see Van Hook et al., 2019). We investigated the properties of these channels by making whole-cell patch recordings from $Cx36^{-/-}$ cones. These recordings were made with a Cs^+ internal (pipette) solution, which contained both Cs^+ and TEA in sufficient concentrations to block K^+ channels (see Materials and methods and Yellen, 1984; Cecchi et al., 1987).

In control Ames' medium, a voltage step from –50 mV to –30 mV elicited a large inward current followed by an outward current (Fig. 2 A). Because previous experiments have indicated that photoreceptors express Ca^{2+}-activated Cl^- currents (Barnes and Hille, 1989; Yagi and Macleish, 1994; Verweij et al., 2003; Lalonde et al., 2008; Stöhr et al., 2009), we repeated the experiment of Fig. 2 A in the presence of external NFA to block the Cl^- channels. When 250 µM NFA was added to the bath solution, the inward current was similar to that in Fig. 2 A, but the outward component of current was largely suppressed (Fig. 2 B). If instead of NFA the retina was perfused with ISR, both inward and outward current components were blocked (Fig. 2 C).

We characterized both the Ca^{2+} conductance and the Ca^{2+}-activated Cl^- current ($i_{Cl(Ca)}$) with the following protocol. The V_m was first held at V_m = –70 mV and stepped to –60 mV, which produced a nearly ohmic increase in current subsequently used in leak subtraction. Voltage steps were then given from V_m = –70 mV to voltages ranging from –50 mV to 0 mV in 10-mV increments. Currents were recorded with a Cs internal (pipette) solution in Ames' medium (Fig. 2 A) and in Ames' with NFA (Fig. 2 B). We used initially 250 µM NFA, but in later experiments, the concentration was reduced to 200 µM without altering the result.

Ca^{2+} currents recorded in the presence of NFA are illustrated in Fig. 2 E, and mean current values with SEM are given in the lower graph of Fig. 2 F (blue). This current is likely to be produced largely if not entirely by $Ca_V1.4$ channels (see Van Hook et al., 2019) and is much larger than the Ca^{2+} current recorded from rods (see for example Wang et al., 2017). The current reached a maximal value of –60 ± 4 pA when the holding potential was between –30 and –20 mV (Fig. 2 F, blue filled squares), and it showed only partial inactivation, maintaining almost 60% of its peak for over 750 ms (Fig. 2 F, blue open squares; averages taken at times indicated by the horizontal black bar above the traces in Fig. 2 E). The waveform and voltage dependence are in satisfactory agreement with other measurements from mouse cones made under somewhat different conditions (Grassmeyer et al., 2019).

Isolation of $i_{Cl(Ca)}$ was achieved by subtracting the current traces recorded in the presence of NFA (Fig. 2 B) from those recorded in its absence (Fig. 2 A). The maximum current averaged from the last 50 ms of the voltage step is plotted in the upper graph of Fig. 2 F (red) for comparison with the voltage-gated Ca^{2+} current i_{Ca}. The peak value of $i_{Cl(Ca)}$ was +48 ± 5 pA at –10 mV and nearly mirrored the voltage dependence of the Ca^{2+} current. Neither i_{Ca} nor $i_{Cl(Ca)}$ was affected by perfusion of 100 µM DL-*threo*-β-benzyloxyaspartic acid (Tocris) to block the Cl^- current of the photoreceptor glutamate transporter (Grassmeyer et al., 2019).

The waveforms of $i_{Cl(Ca)}$ were fit with exponential functions to derive time constants for activation and deactivation, namely

$$i = i_{max}\left(1 - e^{-t/\tau}\right) \tag{1}$$

for activation, and

$$i = i_{max}\left(e^{-t/\tau}\right) \tag{2}$$

for deactivation, where i is the value of the current, i_{max} is the maximum value of i, t is the time, and τ is the time constant.

Ingram et al.
Conductances of mouse cone photoreceptors

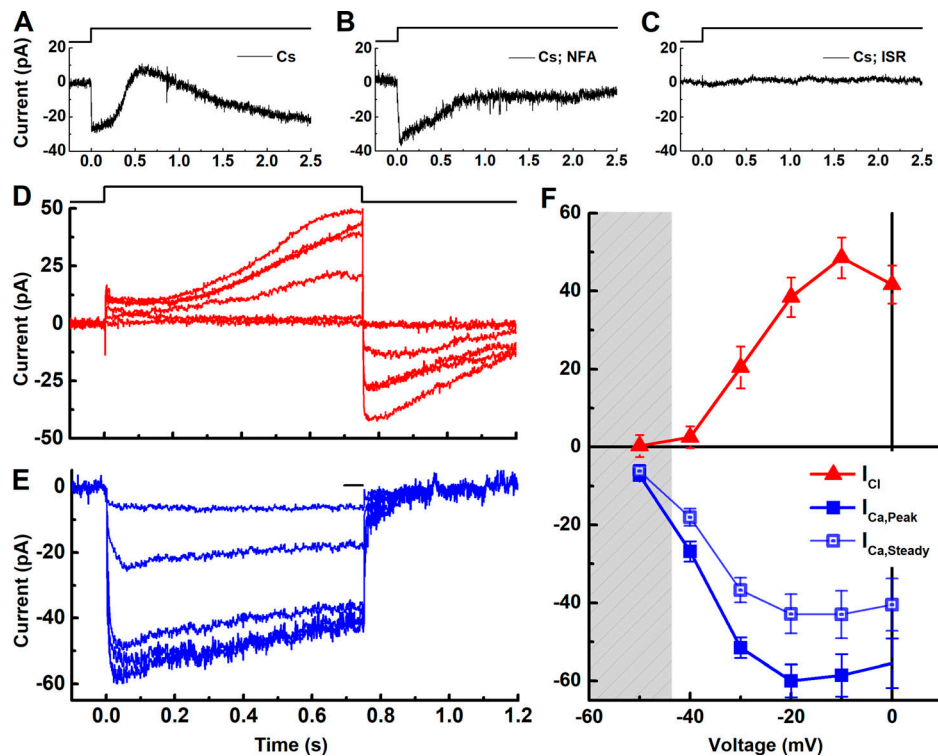Journal of General Physiology
https://doi.org/10.1085/jgp.201912520

4 of 11

Figure 2. Voltage-gated Ca²⁺ and Ca²⁺-activated Cl⁻ currents. Whole-cell patch recordings from $Cx36^{-/-}$ cones. Recordings were made with a Cs⁺ internal (pipette) solution, which contained both Cs⁺ and TEA in sufficient concentrations to block BK channels (see Materials and methods). **(A–C)** Representative, leak-subtracted examples from single cones. **(A)** In the absence of light stimulation, the depolarization from a holding potential of –50 mV to –30 mV (see command monitor above plot) produced an inward current followed by an outward component. **(B)** As in A but with the addition of 200 or 250 µM NFA to the external solution to block the calcium-activated chloride conductance. **(C)** As in A but with the addition of 10 µM ISR to the external solution to block the voltage-gated Ca²⁺ conductance. **(D)** Isolated calcium-activated chloride currents were averaged from 11 cones. Currents were isolated by recording responses to voltage steps as in A and B and then subtracting current traces recorded with NFA from those recorded without NFA. Cones were held at –70 mV before stepping for 750 ms to depolarizing V_ms from –50 mV to 0 mV in 10 mV increments and then returning to –70 mV (see command pulse above plot). **(E)** i_{Ca} was isolated by recording in NFA as in B with the same voltage protocol as in D. Responses to voltage steps from –50 mV to 0 mV in 10-mV increments were leak subtracted and averaged (n = 16). **(F)** Peak and steady-state currents (mean ± SEM) at each voltage from D and E were used to derive the current–voltage relationship of mouse cone $i_{Cl(Ca)}$ shown above (red triangles) and i_{Ca} shown below (filled blue squares, peak current; open blue squares, steady-state current). Shaded area indicates approximate physiological range of membrane voltages.

Activation time constants decreased with strong depolarization from 270 ± 52 ms at –30 mV to 140 ± 9 ms at +10 mV. They likely reflect at least in part the time course of increase of Ca²⁺ concentration in the synaptic terminal. The deactivation time constant (measured from the tail currents at the cessation of the voltage pulse) averaged 280 ± 17 ms and did not appear to depend on the value of the previous voltage step. Its value may reflect the time constant of Ca²⁺ removal by the Ca²⁺-ATPase at the synaptic pedicle (Krizaj and Copenhagen, 1998; Morgans et al., 1998; Cia et al., 2005).

Blocking transduction with GTP-γ-S
The experiments of Figs. 1 and 2 indicate that mouse cones have a voltage-gated Ca²⁺ conductance, which can be gated by voltage steps as well as by light, probably via feedback from horizontal cells. To isolate this feedback component of the response, we included 2 mM GTP-γ-S in our pipette solutions. GTP-γ-S binds nearly irreversibly to the guanosine-nucleotide binding site of the G protein transducin and has been shown to produce a persistent closure of the light-sensitive channels, effectively blocking the photoresponse of the cone from which our

recording was made (see for example Matthews et al., 1996). Our hope was that blocking the outer segment current would reveal any response produced by transduction in neighboring photoreceptors feeding back through horizontal cells onto the cone from which we were recording.

The effect of GTP-γ-S is shown for three representative $Cx36^{-/-}$ cones in Fig. 3 A. After formation of the whole-cell recording, there was a gradual decline of the resting dark current and a concomitant decrease in the amplitude of the photoresponse. At a holding potential of –50 mV near the resting V_m of the $Cx36^{-/-}$ cones (–45.2 ± 1.5 mV, see Ingram et al., 2019), the photoresponse seemed to disappear almost entirely. In a few cells, however, we noticed a small but consistent "wiggle" in the current at V_m = –50 mV, apparently produced by light stimulation. When the holding potential was shifted to more depolarized values, the wiggle became significantly larger (Fig. 3 B). At a holding potential of –30 mV, the light flash consistently produced a small, biphasic current response, which was completely suppressed by the addition of the i_{Ca} blocker ISR (Fig. 3 C).

We reasoned that the biphasic nature of the response could be due to activation of at least two separate channels. Although
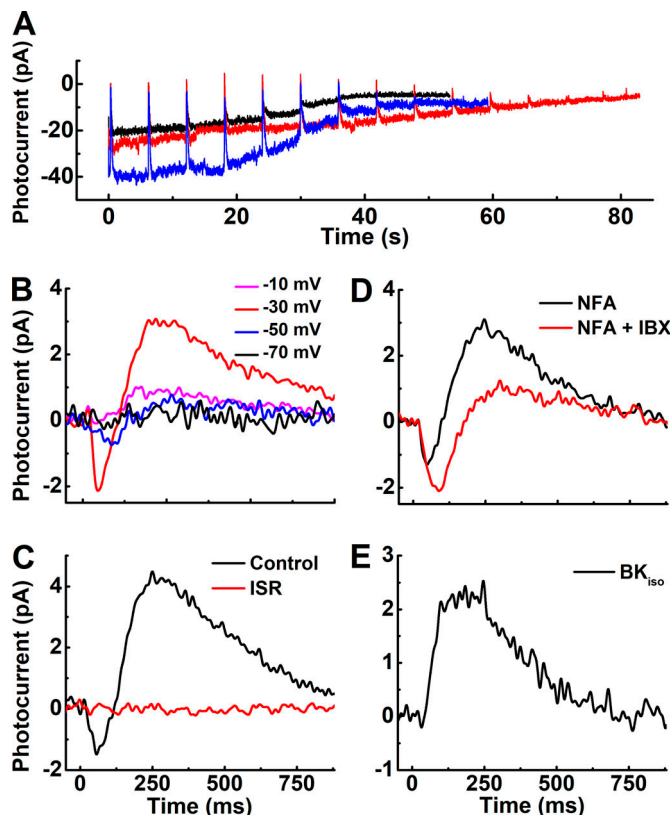
Figure 3. **Feedback-mediated currents elicited by light after dialysis of GTP-γ-S. (A)** Examples from three different cones from *Cx36*^{−/−} mice show the effect of introducing 2 mM GTP-γ-S from the whole-cell patch pipette into the cone cell body. Currents were recorded at a holding potential of $V_m = -50$ mV. GTP-γ-S produced a slow decrease in resting current and nearly eliminated responses to a repeated saturating flash stimuli (1.2×10^4 P*). **(B)** After cones treated as in A had reached a steady-state resting current with little or no response at $V_m = -50$, responses were recorded to the same light stimulus at holding potentials from −70 to −10 mV in steps of 20 mV. Records show baseline-subtracted averages of 13 cones. A strong biphasic response was detected when cones were held at −30 mV (red). **(C)** Responses as in B at a holding potential of −30 mV, with (red) and without (control, black) 10 µM ISR ($n = 2$). **(D)** Responses as in B and C but first with 200 µM NFA in the bath (black, $n = 4$) followed by NFA together with 100 nM IBX (red, $n = 4$). **(E)** Responses from D were subtracted [NFA − (NFA + IBX)] to give IBX-sensitive BK current ($n = 4$). For B–E, flashes were given at t = 0.

application of 200 µM NFA to block $i_{Cl(Ca)}$ had little effect on the waveform of the biphasic response (Fig. 3 D, black trace), much of the positive component of current could be blocked by IBX (Galvez et al., 1990), a blocker of BK-type K⁺ channels (Fig. 3 D, red trace). The responses before and after IBX application were subtracted to isolate the BK component (Fig. 3 E). For i_{Ca} (Fig. 3 D, red trace), the maximum amplitude was −2.5 ± 1.2 pA and the time to peak 87 ± 9 ms ($n = 4$); and for $i_{K(Ca)}$, the maximum amplitude was 3.3 ± 1.5 pA and the time to peak 120 ± 22 ms ($n = 4$).

Hyperpolarization-activated CNG channels
Both rods and cones have been shown to express hyperpolarization-activated CNG (HCN) channels, which produce a mixed Na⁺/K⁺ cationic current called i_h (see Van Hook et al., 2019). This current is

activated by hyperpolarization during the photoresponse and can produce a delayed depolarizing transient often referred to as the "nose" (see for example Fain et al., 1978; Pahlberg et al., 2017). To characterize this conductance in mouse cones, we changed the V_m from $V_m = -50$ mV to values from −25 mV to −135 mV in steps of 10 mV. We included ISR and TEA in the bath solution to block activation of calcium and potassium currents during the voltage steps.

The results of these recordings after leak subtraction are given in Fig. 4 A. The steady-state current values were averaged from the last 50 ms of each stimulus (black bar) and are plotted as a function of step potential as the black symbols and line in Fig. 4 D. The rising phase of each current trace was fit with Eq. 1 to derive a time constant for activation (Fig. 4 A, colored lines). The values of the time constants are given in Fig. 4 B and decreased from ~25 ms near the resting potential of the cone to <10 ms with stronger hyperpolarization.

To measure the reversal potential of i_h, the cone membrane voltage was first stepped from the resting holding potential of −50 mV to −120 mV for 400 ms to activate the conductance and open a substantial fraction of the channels (Fig. 4 C). This step was then followed by a second 400-ms step, depolarizing the V_m to values from −100 mV to +10 mV in intervals of 10 mV. This second step produced the tail currents shown in Fig. 4 C. From these data, we measured the difference in the current 5 ms after the beginning of the depolarizing step (vertical dashed red line to left) and at steady state 250 ms after the beginning of the step (vertical dashed red line to right). This procedure was adopted to compensate for a small leakage current, evident in the current recorded at 250 ms after the second step at positive potentials, where i_h would be expected to be zero. The values of the current difference for voltages near the reversal potential are plotted as the red symbols and line in Fig. 4 D. From these data, we estimated the reversal potential as the potential at which the difference current was zero, giving a value of −28 ± 1.2 mV ($n = 10$). Assuming that the HCN channels are permeable only to monovalent cations, we calculated a relative permeability ratio of sodium to potassium P_{Na}/P_K of ~0.4, similar to that measured in other species (Hestrin, 1987; Barnes and Hille, 1989; Yagi and Macleish, 1994; Demontis et al., 2002; Cia et al., 2005).

Voltage-gated K⁺ conductances
We identified a transient potassium current ($i_{k,trans}$) with the same application of ISR and TEA as in Figs. 1 and 4. This conductance was activated at holding potentials positive of −10 mV and was determined to be an outwardly rectifying conductance (Fig. 5, A and C, black). It peaked 5–10 ms after the initiation of the depolarizing step and relaxed within several hundred milliseconds. A similar waveform and voltage dependence was obtained by subtracting currents in the presence and absence of 2 mM 4-AP to isolate $i_{k,trans}$ (Yagi and Macleish, 1994). In addition to $I_{k,trans}$, a sustained potassium $i_{k,sus}$ channel was isolated by subtraction with and without TEA (Fig. 5 B). The $i_{k,sus}$ was activated with a nearly linear voltage dependence at physiological holding potentials and was maximal at potentials positive of 0 mV (Fig. 5 C, red). It resembles the sustained K⁺ currents previously recorded from salamander (Beech and Barnes, 1989) and primate photoreceptors (Gayet-Primo et al., 2018).
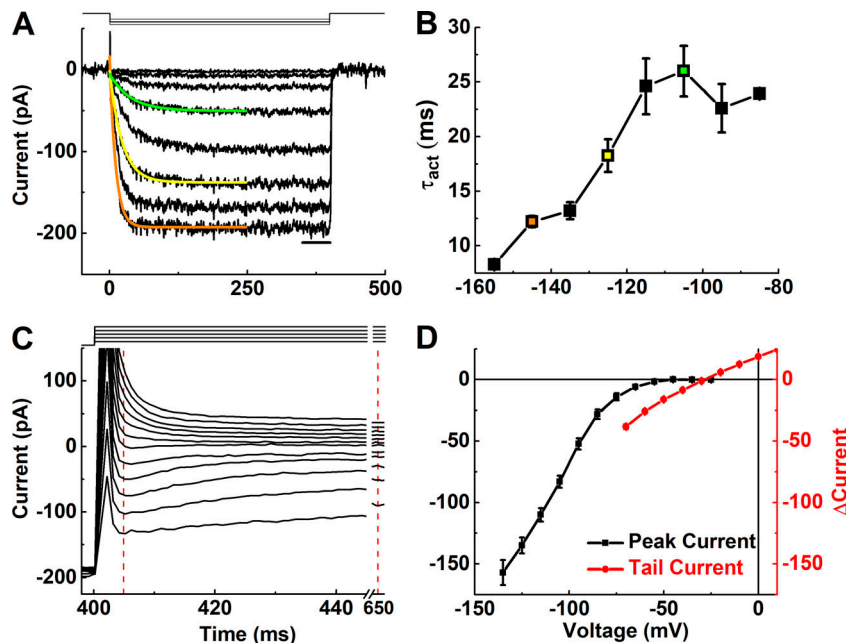
Figure 4. **i_h (HCN channels).** Whole-cell patch recordings from $Cx36^{-/-}$ cones with 25 mM TEA and 10 µM ISR included in the bath solution. The pipette solution was K-Asp. **(A)** Currents from a sample cone held at −50 mV and stepped for 400 ms to potentials of −25 to −135 mV in increments of 10 mV. Responses to depolarizing steps were omitted. Colored lines are fits to single exponential functions to give activation time constants, τ_{act}. See text. **(B)** Values of τ_{act} (mean ± SEM, $n = 10$) from fits like those in A are plotted against holding potential. **(C)** The reversal potential of i_h was measured by first hyperpolarizing the cone from the resting holding potential of −50 mV to −120 mV for 400 ms to activate the conductance, and then depolarizing from −120 mV for another 400 ms to potentials ranging from −100 mV to +10 mV in increments of 10 mV. See command trace above plot. Cones were returned to −50 mV after the second command step. Dashed lines indicate 5 ms and 250 ms after the second voltage step was applied. **(D)** The peak values of the currents were plotted as a function of V_m to derive the current–voltage relationship of mouse cone i_h (black, $n = 10$). The peak current values were averaged from last 50 ms of each voltage step, shown as the thin horizontal bar below the current traces in A. To derive the reversal potential of i_h, we measured the difference in the current just after the beginning of the depolarizing step (vertical dashed red line to left) and at steady-state 250 ms after the beginning of the step (vertical dashed red line to right). This procedure was adopted to compensate for the small leakage current, evident in the nonzero values of current recorded at 250 ms after the second step at positive potentials, where i_h would be expected to be zero. The values of the current differences for voltages near the reversal potential are plotted as the red symbols and line. Data are means ± SEM.

Discussion

We have previously shown that dark-adapted mouse cones in retinal slices can be voltage clamped and retain robust dark currents and photoresponses (Ingram et al., 2019). We have used this preparation to make the first measurements of the voltage dependence of a mammalian photoreceptor light-dependent conductance. We show that the CNG channels in mouse cones have a reversal potential similar to the CNG channels of amphibian and fish photoreceptors, but that the current–voltage curve shows little voltage dependence of conductance within the physiological range. We have used our preparation to characterize cone voltage-gated and Ca²⁺-activated conductances. We show that the voltage-gated Ca²⁺ current i_{Ca} is greatest at $V_m = $ −20 to −30 mV and incompletely inactivates, retaining ~60% of peak current at steady-state. Entry of Ca²⁺ evokes a large Ca²⁺-activated Cl⁻ current whose voltage dependence mirrored that of i_{Ca}. Dialysis of GTP-γ-S into the cone to block outer-segment CNG channels revealed a light-evoked response consisting of a small inward Ca²⁺ current followed by gating of Ca²⁺-activated K⁺ channels, presumably produced via feedback from neighboring horizontal cells. We identified and characterized the cone HCN or i_h current, which is activated by membrane hyperpolarization; we measured its voltage dependence, kinetics, and relative cation permeability. Finally, we isolated and identified several different K⁺ conductances, including a Ca²⁺-activated BK current blocked by IBX (Fig. 3, D and E); a transient, outwardly rectifying $i_{k,trans}$, sensitive to 4-AP and activated by strong depolarization (Fig. 5, A and C); and a more sustained voltage-gated potassium current, $i_{k,sus}$, which is active at physiological membrane voltages and blocked by TEA (Fig. 5, B and C), similar to the i_{KX} of salamander rods (Beech and Barnes, 1989) and the $K_V8.2/K_V2$ current of primate photoreceptors (Gayet-Primo et al., 2018).

Comparison to previous results

Our measurements of the voltage dependence of the light-dependent current in mouse cones are similar to those from bass (fish) cones (Miller and Korenbrot, 1993) but differ in some important respects from previous recordings from amphibian rods (Baylor and Nunn, 1986). Although we report a similar reversal potential presumably indicating a similar relative ion permeability (Fig. 1 F), the voltage dependence of the current–voltage curve is different. This curve measured from amphibian rods is nonlinear and outwardly rectifying within the physiological range, apparently at least in part the result of divalention block of the CNG channels (see Yau and Baylor, 1989). In contrast, measurements in mouse and bass cones indicate that this curve is nearly linear within the physiological range. This difference is important, because the nonlinearity of the salamander rod i-V curve has the consequence that current responses recorded with suction electrodes are nearly identical with and without voltage clamp (Baylor and Nunn, 1986). This is because the change in current produced by light stimulation is given by

$$\Delta i = \Delta g(V_m - E_{rev}), \qquad (3)$$

where Δi is the change in current produced by the closing of the outer-segment CNG channels, Δg is the change in conductance of the channels, and E_{rev} is the reversal potential of the channels. The value of Δg is given by the ratio of the change in current to the driving force ($V_m - E_{rev}$) and is the change in chord conductance. For a salamander rod, the voltage dependence of the
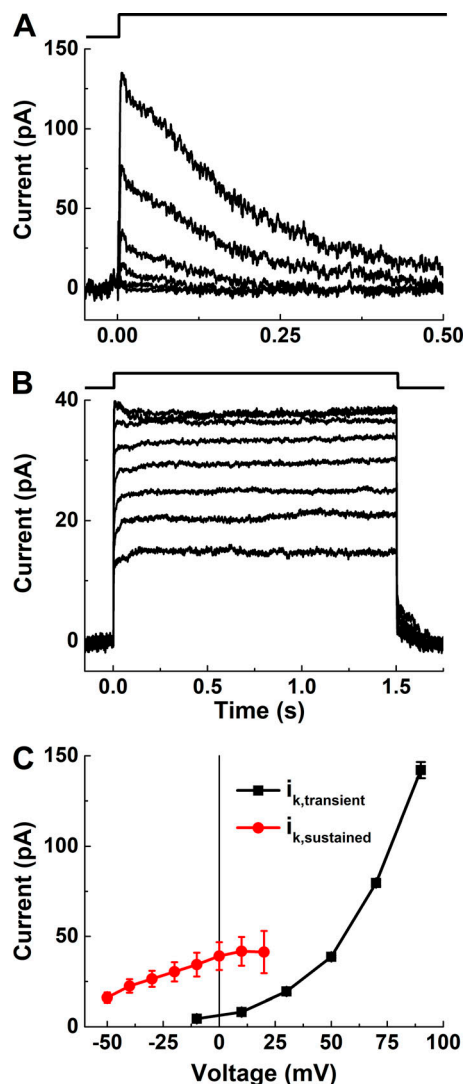
Ingram et al.
Conductances of mouse cone photoreceptors

Journal of General Physiology 7 of 11
https://doi.org/10.1085/jgp.201912520

Figure 5. **Voltage-gated K+ currents.** Whole-cell patch recordings from *Cx36−/−* cones. **(A)** Voltage-gated transient current ($i_{k,trans}$) recorded in the presence of 25 mM TEA to block a sustained current, together with 10 μM ISR to block Ca^{2+} currents and Ca^{2+}-activated K+ and Cl− currents. Recordings are average responses (after leak subtraction, $n = 5$) to voltage steps from a holding potential of $V_m = −70$ mV to voltages from −50 mV to +20 mV in steps of 10 mV. **(B)** Sustained, TEA-sensitive component of K+ current ($i_{k,sus}$) isolated by recording responses to voltage steps in the presence and absence of TEA. Currents were recorded in external Ames' medium containing 10 μM ISR, 7.5 mM CsCl, and 2 mM 4-AP, with and without 25 mM TEA. Cones were stimulated with steps from a holding potential of $V_m = −50$ mV to voltages from −10 mV to +90 mV in steps of 20 mV. Records with TEA were subtracted from those without TEA. Average current traces are shown from eight cones. **(C)** Means ± SEM of peak currents from A and B are plotted as a function of step voltage. Transient currents from A are plotted in black ($n = 5$), and sustained currents in red ($n = 8$).

chord conductance has the effect that, in the absence of voltage clamp, the increase in driving force during the photoresponse is nearly compensated by the voltage-dependent decrease in chord conductance, so that the light-dependent change in current is nearly independent of voltage. For mouse cones, on the other hand, the change in current increases as V_m becomes more negative, so that responses recorded with suction electrodes in

unclamped photoreceptors less accurately reflect the amplitude and time course of changes in outer-segment conductance than do voltage-clamp recordings. In addition, the high capacitance of mouse cones resulting from the open lamellae of the outer-segment plasma membrane would tend to retard the initial time course of the photoresponse recorded with suction electrodes, as was previously demonstrated for cones in salamander (Perry and McNaughton, 1991). These considerations argue that accurate measurements of the amplitude and kinetics of changes in the cone outer-segment CNG conductance are best made with voltage clamp.

Our measurements characterizing major inner-segment conductances largely agree with previous studies from other vertebrate species (see Van Hook et al., 2019). We affirm the presence of an HCN or i_h current activated by hyperpolarization and permeable to both Na+ and K+, consistent with the expression of the HCN channels by photoreceptors (Moosmang et al., 2001; Müller et al., 2003). Additionally, our measurements of i_{Ca} are comparable to those recently made by Grassmeyer et al. (2019) in both amplitude and voltage dependence. The calcium-activated and voltage-gated conductances we have recorded also have similar properties to those investigated previously (Barnes and Hille, 1989; Xu and Slaughter, 2005; Pelucchi et al., 2008; Stöhr et al., 2009), including in primates (Verweij et al., 2003; but see Yagi and Macleish, 1994). These Ca^{2+}-activated Cl− and K+ currents would tend to stabilize the V_m during changes in Ca^{2+} current and transmitter release, as others have previously argued (Lalonde et al., 2008).

Light response after blocking outer-segment channels

We show that, in a slice preparation, light produces a current even after dialysis of GTP-γ-S to block the outer-segment CNG channels (Fig. 3). Little or no response was seen at hyperpolarized V_ms ($V_m < −50$ mV), where the driving force for the CNG channels would have been large. This observation indicates that current from the CNG channels is unlikely to have made any significant contribution to the response. We believe that this remaining photoresponse is initiated by a change in i_{Ca} for the following reasons. The response was voltage-dependent and was maximal when i_{Ca} was maximal (Fig. 3 B). It was blocked completely with the L-type Ca^{2+} channel blocker ISR (Fig. 3 C). Only in the presence of ISR have we been able to record a reversal potential for the CNG channels consistent with previous recordings from photoreceptors and in vitro measurements of the relative ion permeabilities (Fig. 1 E). We hypothesize that the increase in Ca^{2+} current is produced by feedback from horizontal cells in our retinal slice, resulting from a change in extracellular pH, which then alters the amplitude and voltage dependence of the Ca^{2+} conductance (see Thoreson and Mangel, 2012). The amplitude of this change in Ca^{2+} current may represent a lower bound, given the limitations of the slice preparation and probable decrease in horizontal-cell activity.

Previous measurements of the voltage dependence of the photoreceptor light-dependent conductance were made on single photoreceptors, which were mechanically isolated from the retina (Baylor and Nunn, 1986; Miller and Korenbrot, 1993), or from membrane patches (Haynes and Yau, 1985). Isolated photoreceptors often lack synaptic terminals and would not have

associated horizontal-cell feedback onto the photoreceptors. This may explain why pharmacological isolation was necessary for the determination of the reversal potential of the photoresponse in mouse cones but not in these other experiments. Though our slice preparation introduces the additional complication of photoreceptor connections to other retinal cells, it maintains the structural integrity of the photoreceptor and preserves responsivity to light (Cao et al., 2008; Okawa et al., 2010), which had not been possible in previous experiments characterizing membrane conductances of mammalian rods and cones.

Contribution of electrogenic transporters

Although it is conceivable that Na^+/K^+-Ca^{2+} exchange (NCKX) and an excitatory amino acid transporter (EAAT) would have contributed to the currents we have measured, we think it unlikely that either transporter influenced the value of the reversal potential of the light-activated conductance. The current from NCKX exchange contributes to the initial waveform of the photoresponse as the CNG channels close (see for example Hodgkin et al., 1987; Perry and McNaughton, 1993). Because light-induced changes in Ca^{2+} occur more quickly in the outer segments of cones than in rods (Perry and McNaughton, 1993; Sampath et al., 1999), the NCKX current would be expected to have a rapid time course and to have little effect on the peak amplitude of saturating photoresponses, like those in Fig. 1. As evidence for this claim, we adduce the response of the cone near the reversal potential in Fig. 1 D. There is little indication of a discontinuity in the initial waveform of the response, which might indicate a contribution of NCKX exchange. The amplitude of the NCKX current in salamander cones is ~10% of the current through the CNG channels (Perry and McNaughton, 1991), and model calculations suggest that it has a comparable amplitude in mouse (J. Reingruber, personal communication).

EAATs have been proposed to remove glutamate from the photoreceptor synaptic cleft and to have a critical role in the transmission of the photoresponse (Szmajda and Devries, 2011; Tse et al., 2014). Photoreceptors have been reported to express EAATs (Reye et al., 2002; Hasegawa et al., 2006), which can activate to increase membrane permeability to anions and produce a large change in current during glutamate reuptake from the synaptic cleft (see for example Grassmeyer et al., 2019). We think it unlikely that an EAAT current could have contributed to our measurements of reversal potential in Fig. 1, C and D, because these experiments were performed in the presence of ISR, which blocks the cone Ca^{2+} current at the synapse and prevents any glutamate release. This was also true for recordings of i_h in Fig. 4. Measurements of Ca^{2+} and Ca^{2+}-activated Cl^- currents like those in Fig. 3 were repeated in the presence of 100 µM DL-*threo*-β-benzyloxyaspartic acid to block the glutamate transporter, with no effect on the recorded currents. We therefore think it unlikely that EAATs made any significant contribution to the data we have reported.

Physiological significance

Cones are much less abundant than rods in most mammalian retinas, including humans, but they are primarily responsible for light detection in daylight and largely determine our visual behavior under most conditions of illumination. Much less is known about cones than about rods, because of the greater difficulty of studying cone biochemistry and physiology. We have chosen to focus our efforts on mouse because of the large number of animals presently available with mutations in critical proteins. Most of the data in this paper were, for example, recorded from retinas lacking Cx36 gap junctions to eliminate current flow between photoreceptors, thus improving the space clamp and accuracy of our measurements. Only for mouse are $Cx36^{-/-}$ animal lines presently available. Other mouse lines have also been isolated with mutations in essential transduction enzymes, such as the guanylyl cyclase-activating proteins and recoverin (Ingram et al., 2019). Our methods should now make possible a detailed investigation of cone phototransduction in this species.

Voltage-clamp recordings will permit a quantitative study of the sensitivity and kinetics of the light-dependent change in outer-segment conductance with greater accuracy than would be possible with suction-electrode recording. Accurate measurements of changes in outer-segment conductance will be essential in any attempt to model the cone photoresponse. Only with the greater frequency response of voltage clamp will we be able to understand changes in the kinetics of the cone photoresponse in background light. Our characterization of the time and voltage dependence of inner-segment conductances will help us understand how these processes shape the cone photovoltage. Mice are presently available with deletions of each of the voltage-dependent and Ca^{2+}-activated conductances we have shown to be present in the cone inner segment. Recordings from these mutant animals may help us understand the role of each inner-segment conductance in producing the photovoltage that is communicated to the cone synaptic terminal, which is the primary response signaling light detection to the rest of the nervous system.

Once we have a complete characterization of the time and intensity dependence of the outer-segment conductance, together with the voltage dependence and kinetics of each of the inner-segment conductances, we should be able to provide an accurate model of the light response of mouse cones. Although we have known for over 40 yr that photoreceptors express a variety of channels permeable to different ions, we have lacked the tools to analyze in detail what each channel type does. Such information will undoubtedly provide new insight into mechanisms of perception particularly for daylight vision, which makes the greatest contribution to our visual behavior.

References

Ames, A. III, and F.B. Nesbett. 1981. In vitro retina as an experimental model of the central nervous system. *J. Neurochem.* 37:867–877. https://doi.org/10.1111/j.1471-4159.1981.tb04473.x

Arshavsky, V.Y., and M.E. Burns. 2012. Photoreceptor signaling: supporting vision across a wide range of light intensities. *J. Biol. Chem.* 287:1620–1626. https://doi.org/10.1074/jbc.R111.305243

Barnes, S., and B. Hille. 1989. Ionic channels of the inner segment of tiger salamander cone photoreceptors. *J. Gen. Physiol.* 94:719–743. https://doi.org/10.1085/jgp.94.4.719

Baylor, D.A., and B.J. Nunn. 1986. Electrical properties of the light-sensitive conductance of rods of the salamander Ambystoma tigrinum. *J. Physiol.* 371:115–145. https://doi.org/10.1113/jphysiol.1986.sp015964

Beech, D.J., and S. Barnes. 1989. Characterization of a voltage-gated K+ channel that accelerates the rod response to dim light. *Neuron.* 3:573–581. https://doi.org/10.1016/0896-6273(89)90267-5

Calvert, P.D., N.V. Krasnoperova, A.L. Lyubarsky, T. Isayama, M. Nicoló, B. Kosaras, G. Wong, K.S. Gannon, R.F. Margolskee, R.L. Sidman, et al. 2000. Phototransduction in transgenic mice after targeted deletion of the rod transducin alpha-subunit. *Proc. Natl. Acad. Sci. USA.* 97:13913–13918. https://doi.org/10.1073/pnas.250478897

Cao, Y., H. Song, H. Okawa, A.P. Sampath, M. Sokolov, and K.A. Martemyanov. 2008. Targeting of RGS7/Gbeta5 to the dendritic tips of ON-bipolar cells is independent of its association with membrane anchor R7BP. *J. Neurosci.* 28:10443–10449. https://doi.org/10.1523/JNEUROSCI.3282-08.2008

Cecchi, X., D. Wolff, O. Alvarez, and R. Latorre. 1987. Mechanisms of Cs+ blockade in a Ca2+-activated K+ channel from smooth muscle. *Biophys. J.* 52:707–716. https://doi.org/10.1016/S0006-3495(87)83265-4

Choi, S.Y., S. Jackman, W.B. Thoreson, and R.H. Kramer. 2008. Light regulation of Ca2+ in the cone photoreceptor synaptic terminal. *Vis. Neurosci.* 25:693–700. https://doi.org/10.1017/S0952523808080814

Cia, D., A. Bordais, C. Varela, V. Forster, J.A.J. Sahel, A. Rendon, and S. Picaud. 2005. Voltage-gated channels and calcium homeostasis in mammalian rod photoreceptors. *J. Neurophysiol.* 93:1468–1475. https://doi.org/10.1152/jn.00874.2004

Copenhagen, D.R., and C.E. Jahr. 1989. Release of endogenous excitatory amino acids from turtle photoreceptors. *Nature.* 341:536–539. https://doi.org/10.1038/341536a0

Deans, M.R., B. Volgyi, D.A. Goodenough, S.A. Bloomfield, and D.L. Paul. 2002. Connexin36 is essential for transmission of rod-mediated visual signals in the mammalian retina. *Neuron.* 36:703–712. https://doi.org/10.1016/S0896-6273(02)01046-2

Demontis, G.C., A. Moroni, B. Gravante, C. Altomare, B. Longoni, L. Cervetto, and D. DiFrancesco. 2002. Functional characterisation and subcellular localisation of HCN1 channels in rabbit retinal rod photoreceptors. *J. Physiol.* 542:89–97. https://doi.org/10.1113/jphysiol.2002.017640

DeVries, S.H., and E.A. Schwartz. 1999. Kainate receptors mediate synaptic transmission between cones and 'Off' bipolar cells in a mammalian retina. *Nature.* 397:157–160. https://doi.org/10.1038/16462

Diamond, J.S. 2017. Inhibitory Interneurons in the Retina: Types, Circuitry, and Function. *Annu. Rev. Vis. Sci.* 3:1–24. https://doi.org/10.1146/annurev-vision-102016-061345

Fain, G.L. 2019. Sensory Transduction. Second edition. Oxford University Press, Oxford. https://doi.org/10.1093/oso/9780198835028.001.0001

Fain, G.L., and A.P. Sampath. 2018. Rod and cone interactions in the retina. *F1000Research.* 7(F1000 Faculty Rev):657. doi:https://doi.org/10.12688/f1000research.14421.1.eCollection2018.

Fain, G.L., F.N. Quandt, B.L. Bastian, and H.M. Gerschenfeld. 1978. Contribution of a caesium-sensitive conductance increase to the rod photoresponse. *Nature.* 272:466–469. https://doi.org/10.1038/272467a0

Galvez, A., G. Gimenez-Gallego, J.P. Reuben, L. Roy-Contancin, P. Feigenbaum, G.J. Kaczorowski, and M.L. Garcia. 1990. Purification and characterization of a unique, potent, peptidyl probe for the high conductance calcium-activated potassium channel from venom of the scorpion Buthus tamulus. *J. Biol. Chem.* 265(19):11083–11090. .

Gayet-Primo, J., D.B. Yaeger, R.A. Khanjian, and T. Puthussery. 2018. Heteromeric $K_V2/K_V8.2$ Channels Mediate Delayed Rectifier Potassium Currents in Primate Photoreceptors. *J. Neurosci.* 38:3414–3427. https://doi.org/10.1523/JNEUROSCI.2440-17.2018

Grassmeyer, J.J., A.L. Cahill, C.L. Hays, C. Barta, R.M. Quadros, C.B. Gurumurthy, and W.B. Thoreson. 2019. Ca^{2+} sensor synaptotagmin-1 mediates exocytosis in mammalian photoreceptors. *eLife.* 8:e45946. https://doi.org/10.7554/eLife.45946

Hasegawa, J., T. Obara, K. Tanaka, and M. Tachibana. 2006. High-density presynaptic transporters are required for glutamate removal from the first visual synapse. *Neuron.* 50:63–74. https://doi.org/10.1016/j.neuron.2006.02.022

Haynes, L., and K.W. Yau. 1985. Cyclic GMP-sensitive conductance in outer segment membrane of catfish cones. *Nature.* 317:61–64. https://doi.org/10.1038/317061a0

Hestrin, S. 1987. The properties and function of inward rectification in rod photoreceptors of the tiger salamander. *J. Physiol.* 390:319–333. https://doi.org/10.1113/jphysiol.1987.sp016703

Hodgkin, A.L., P.A. McNaughton, and B.J. Nunn. 1987. Measurement of sodium-calcium exchange in salamander rods. *J. Physiol.* 391:347–370. https://doi.org/10.1113/jphysiol.1987.sp016742

Ingram, N.T., A.P. Sampath, and G.L. Fain. 2019. Voltage-clamp recordings of light responses from wild-type and mutant mouse cone photoreceptors. *J. Gen. Physiol.* 151:1287–1299. https://doi.org/10.1085/jgp.201912419

Jeon, C.-J., E. Strettoi, and R.H. Masland. 1998. The major cell populations of the mouse retina. *J. Neurosci.* 18:8936–8946. https://doi.org/10.1523/JNEUROSCI.18-21-08936.1998

Johnson, J.E. Jr., G.A. Perkins, A. Giddabasappa, S. Chaney, W. Xiao, A.D. White, J.M. Brown, J. Waggoner, M.H. Ellisman, and D.A. Fox. 2007. Spatiotemporal regulation of ATP and Ca2+ dynamics in vertebrate rod and cone ribbon synapses. *Mol. Vis.* 13:887–919.

Kaupp, U.B., and R. Seifert. 2002. Cyclic nucleotide-gated ion channels. *Physiol. Rev.* 82:769–824. https://doi.org/10.1152/physrev.00008.2002

Krizaj, D., and D.R. Copenhagen. 1998. Compartmentalization of calcium extrusion mechanisms in the outer and inner segments of photoreceptors. *Neuron.* 21:249–256. https://doi.org/10.1016/S0896-6273(00)80531-0

Kurahashi, T. 1989. Activation by odorants of cation-selective conductance in the olfactory receptor cell isolated from the newt. *J. Physiol.* 419:177–192. https://doi.org/10.1113/jphysiol.1989.sp017868

Lalonde, M.R., M.E. Kelly, and S. Barnes. 2008. Calcium-activated chloride channels in the retina. *Channels (Austin).* 2:252–260. https://doi.org/10.4161/chan.2.4.6704

Matthews, H.R., M.C. Cornwall, and G.L. Fain. 1996. Persistent activation of transducin by bleached rhodopsin in salamander rods. *J. Gen. Physiol.* 108:557–563. https://doi.org/10.1085/jgp.108.6.557

Miller, J.L., and J.I. Korenbrot. 1993. In retinal cones, membrane depolarization in darkness activates the cGMP-dependent conductance. A model of Ca homeostasis and the regulation of guanylate cyclase. *J. Gen. Physiol.* 101:933–960. https://doi.org/10.1085/jgp.101.6.933

Moosmang, S., J. Stieber, X. Zong, M. Biel, F. Hofmann, and A. Ludwig. 2001. Cellular expression and functional characterization of four hyperpolarization-activated pacemaker channels in cardiac and neuronal tissues. *Eur. J. Biochem.* 268:1646–1652. https://doi.org/10.1046/j.1432-1327.2001.02036.x

Morgans, C.W., O. El Far, A. Berntson, H. Wässle, and W.R. Taylor. 1998. Calcium extrusion from mammalian photoreceptor terminals. *J. Neurosci.* 18:2467–2474. https://doi.org/10.1523/JNEUROSCI.18-07-02467.1998

Müller, F., A. Scholten, E. Ivanova, S. Haverkamp, E. Kremmer, and U.B. Kaupp. 2003. HCN channels are expressed differentially in retinal bipolar cells and concentrated at synaptic terminals. *Eur. J. Neurosci.* 17: 2084–2096. https://doi.org/10.1046/j.1460-9568.2003.02634.x

Neher, E. 1992. Correction for liquid junction potentials in patch clamp experiments. *Methods Enzymol.* 207:123–131. https://doi.org/10.1016/0076-6879(92)07008-C

Nikonov, S.S., R. Kholodenko, J. Lem, and E.N. Pugh Jr. 2006. Physiological features of the S- and M-cone photoreceptors of wild-type mice from single-cell recordings. *J. Gen. Physiol.* 127:359–374. https://doi.org/10.1085/jgp.200609490

Okawa, H., K.J. Miyagishima, A.C. Arman, J.B. Hurley, G.D. Field, and A.P. Sampath. 2010. Optimal processing of photoreceptor signals is required to maximize behavioural sensitivity. *J. Physiol.* 588:1947–1960. https://doi.org/10.1113/jphysiol.2010.188573

Packer, O.S., J. Verweij, P.H. Li, J.L. Schnapf, and D.M. Dacey. 2010. Blue-yellow opponency in primate S cone photoreceptors. *J. Neurosci.* 30: 568–572. https://doi.org/10.1523/JNEUROSCI.4738-09.2010

Pahlberg, J., R. Frederiksen, G.E. Pollock, K.J. Miyagishima, A.P. Sampath, and M.C. Cornwall. 2017. Voltage-sensitive conductances increase the sensitivity of rod photoresponses following pigment bleaching. *J. Physiol.* 595:3459–3469. https://doi.org/10.1113/JP273398

Pelucchi, B., A. Grimaldi, and A. Moriondo. 2008. Vertebrate rod photoreceptors express both BK and IK calcium-activated potassium channels, but only BK channels are involved in receptor potential regulation. *J. Neurosci. Res.* 86:194–201. https://doi.org/10.1002/jnr.21467

Perry, R.J., and P.A. McNaughton. 1991. Response properties of cones from the retina of the tiger salamander. *J. Physiol.* 433:561–587. https://doi.org/10.1113/jphysiol.1991.sp018444

Perry, R.J., and P.A. McNaughton. 1993. The mechanism of ion transport by the Na(+)-Ca2+,K+ exchange in rods isolated from the salamander retina. *J. Physiol.* 466:443–480.

Reye, P., R. Sullivan, E.L. Fletcher, and D.V. Pow. 2002. Distribution of two splice variants of the glutamate transporter GLT1 in the retinas of humans, monkeys, rabbits, rats, cats, and chickens. *J. Comp. Neurol.* 445: 1–12. https://doi.org/10.1002/cne.10095

Sampath, A.P., H.R. Matthews, M.C. Cornwall, J. Bandarchi, and G.L. Fain. 1999. Light-dependent changes in outer segment free-Ca²⁺ concentration in salamander cone photoreceptors. *J. Gen. Physiol.* 113:267–277. https://doi.org/10.1085/jgp.113.2.267

Stöhr, H., J.B. Heisig, P.M. Benz, S. Schöberl, V.M. Milenkovic, O. Strauss, W.M. Aartsen, J. Wijnholds, B.H. Weber, and H.L. Schulz. 2009. TMEM16B, a novel protein with calcium-dependent chloride channel activity, associates with a presynaptic protein complex in photoreceptor terminals. *J. Neurosci.* 29:6809–6818. https://doi.org/10.1523/JNEUROSCI.5546-08.2009

Szmajda, B.A., and S.H. Devries. 2011. Glutamate spillover between mammalian cone photoreceptors. *J. Neurosci.* 31:13431–13441. https://doi.org/10.1523/JNEUROSCI.2105-11.2011

Taylor, W.R., and C. Morgans. 1998. Localization and properties of voltage-gated calcium channels in cone photoreceptors of Tupaia belangeri. *Vis. Neurosci.* 15:541–552. https://doi.org/10.1017/S0952523898153142

Thoreson, W.B., and S.C. Mangel. 2012. Lateral interactions in the outer retina. *Prog. Retin. Eye Res.* 31:407–441. https://doi.org/10.1016/j.preteyeres.2012.04.003

Tse, D.Y., I. Chung, and S.M. Wu. 2014. Pharmacological inhibitions of glutamate transporters EAAT1 and EAAT2 compromise glutamate transport in photoreceptor to ON-bipolar cell synapses. *Vision Res.* 103:49–62. https://doi.org/10.1016/j.visres.2014.07.020

Van Hook, M.J., S. Nawy, and W.B. Thoreson. 2019. Voltage- and calcium-gated ion channels of neurons in the vertebrate retina. *Prog. Retin. Eye Res.* 72:100760. https://doi.org/10.1016/j.preteyeres.2019.05.001

Verweij, J., M. Kamermans, and H. Spekreijse. 1996. Horizontal cells feed back to cones by shifting the cone calcium-current activation range. *Vision Res.* 36:3943–3953. https://doi.org/10.1016/S0042-6989(96)00142-3

Verweij, J., E.P. Hornstein, and J.L. Schnapf. 2003. Surround antagonism in macaque cone photoreceptors. *J. Neurosci.* 23:10249–10257. https://doi.org/10.1523/JNEUROSCI.23-32-10249.2003

Wang, Y., K.E. Fehlhaber, I. Sarria, Y. Cao, N.T. Ingram, D. Guerrero-Given, B. Throesch, K. Baldwin, N. Kamasawa, T. Ohtsuka, et al. 2017. The Auxiliary Calcium Channel Subunit alpha2delta4 Is Required for Axonal Elaboration, Synaptic Transmission, and Wiring of Rod Photoreceptors. *Neuron.* 93:1359–1374.e6.

Xu, J.W., and M.M. Slaughter. 2005. Large-conductance calcium-activated potassium channels facilitate transmitter release in salamander rod synapse. *J. Neurosci.* 25:7660–7668. https://doi.org/10.1523/JNEUROSCI.1572-05.2005

Yagi, T., and P.R. Macleish. 1994. Ionic conductances of monkey solitary cone inner segments. *J. Neurophysiol.* 71:656–665. https://doi.org/10.1152/jn.1994.71.2.656

Yau, K.W., and D.A. Baylor. 1989. Cyclic GMP-activated conductance of retinal photoreceptor cells. *Annu. Rev. Neurosci.* 12:289–327. https://doi.org/10.1146/annurev.ne.12.030189.001445

Yau, K.-W., and R.C. Hardie. 2009. Phototransduction motifs and variations. *Cell.* 139:246–264. https://doi.org/10.1016/j.cell.2009.09.029

Yellen, G. 1984. Ionic permeation and blockade in Ca2+-activated K+ channels of bovine chromaffin cells. *J. Gen. Physiol.* 84:157–186. https://doi.org/10.1085/jgp.84.2.157